Difunctionalized dyes for DSSCs based on two different scaffolds: *p-tert*-butylcalix[4]rene or isophthalic acid.

Isolda Duerto [a], Daniel Barrios [b], Javier Garín [a], Jesús Orduna [a,*], Belén Villacampa [b], María-Jesús Blesa [a,*]

Addresses:

[a] Departamento de Química Orgánica, ICMA
Universidad de Zaragoza-CSIC
50009, Zaragoza (Spain)
E-mail: mjblesa@unizar.es

[b] Departamento de Física de la Materia Condensada, ICMA
Universidad de Zaragoza-CSIC
50009, Zaragoza (Spain)
Addresses:

Corresponding author:

Dr. María-Jesús Blesa: mjblesa@unizar.es

Authors:

Isolda Duerto: isolda@unizar.es
Daniel Barrios: danielb@unizar.es
Prof. Javier Garín: jgarin@unizar.es
Dr. Jesús Orduna: jorduna@unizar.es
Dr. Belén Villacampa: bvillaca@unizar.es

Difunctionalized dyes for DSSCs based on two different scaffolds: isophthalic acid or 4-tert-butylcalix[4]arene

Isolda Duerto [a], Daniel Barrios [b], Javier Garín [a], Jesús Orduna [a,*], Belén Villacampa [b], María-Jesús Blesa [a,*]

Addresses:

[a] Departamento de Química Orgánica, ICMA
Universidad de Zaragoza-CSIC
50009, Zaragoza (Spain)
E-mail: mjblesa@unizar.es

[b] Departamento de Física de la Materia Condensada, ICMA
Universidad de Zaragoza-CSIC
50009, Zaragoza (Spain)

Abstract

Novel DSSCs (Dye Sensitized Solar Cells) have been developed with difunctionalized dyes, which are based on isophthalic acid or *4-tert*-butylcalix[4]arene as scaffoldand *N,N*-dialkylaniline as electrondonor connected to thiophene as π-spacer. This heteroaromatic ring has been used because of its thermal stability and adequate charge transfer. The use of *4-tert*-butylcalix[4]arene has given rise a considerable increase of the molar extinction coefficient in this difunctionalized dye relative to the individual one, which makes them susceptible to be used in low luminosity condition. All dyes have been completely characterized. The photoelectrochemical properties of the devices prepared with or without co-adsorbate (chenodeoxycholic acid) have been determined. When co-adsorbate is added, solar cells prepared with isophthalic acid and *4-tert*-butylcalix[4]arene have power conversion efficiencies of 6.0 and 6.3 %, respectively; such devices also display good long-term stability up to 1000 h.

Keywords
metal-free sensitizer, multichromophore, calix[4]arene, isophthalic acid

1. Introduction

Solar energy is a renewable alternative to face world energy demand. [1] Nowadays this market is dominated by photovoltaic energy from silicon panels. However, DSSCs are an interesting option at both academic and industrial world because of the versatility of the synthesis of dyes and the low cost in cell fabrication compared to cells prepared with silicon based devices. Most common dyes are those prepared with ruthenium [2] and porphyrins, [3] which have not simple synthesis. In addition, devices prepared with ruthenium sensitizers are not environmentally friendly, and this metal is expensive and not abundant. In this context, metal-free sensitizers, with a general structure based on a donor part, a π-spacer and an acceptor (D-π-A) are an alternative. *N, N*-dialkylanilines have been used as donors (D) because of their simple synthesis, light absorption capacity and donor ability and also its charge transfer band appears bathochromically shifted with respect to the triphenylamine derivatives (TPA), commonly used in this field.[4-6] Thiophene, used as π-spacer, is a heteroaromatic ring which combines good charge transfer properties with high thermal stability. [7] The anchor group must allow the transfer of electrons from the dye to the semiconductor. The cyanoacetic acid is commonly used due to its double character as an acceptor and anchor group due to the cyano group which acts as an acceptor (A) and the carboxylic group which causes the linkage to TiO_2 surface.[8]
The control of the aggregation is an important issue because it affects the performance of the DSSC device. The aggregation can be modified by changing the molecular structure of the dye, for example, reducing its molecular planarity [9], including a bulky group [10], or changing the nature [11], and the position [12] of the anchoring group. In addition, the conditions of dye-sensitization can be tuned by adding a co-adsorbent such as CDCA or modifying the time adsorption of the dye on the electrode. [13]
It has been described that double D-A branched dyes with the chromophores connected via non-conjugated alkyl linkages have more intense absorbance (per chromophore unit) as compared to the single one. The use of double branched organic dyes gives rise to an improvement of photovoltaic properties; in particular an increase of the short circuit photocurrent value has been reported [14, 15]. It is expected that the linkage might influence the geometrical configuration of dyes on the TiO_2 films affecting the aggregation and the performance of the device. [16] Double dyes with the alkyl linkage in either the π-bridge part [17] or the donor part were studied by Cao [18] and these studies points out that the alkyl linkage position has an effect on dye adsorption amount, dye aggregation and light harvesting ability. In this field, our research group prepared double systems based on calix[4]arene scaffold with an alkyl linkage in the π – bridge. [19, 20] As far as we know there are no dyes based on calix[4]arene derivatives with an alkyl linkage in the donor part.
Then in this work we will study the photophysical and photovoltaic properties of dyes based on calix[4]arene derivatives linked by the aniline moiety which acts as donor part (D), a thiophene as π-spacer (π) and cyanoacetic as acceptor (A). The isophthalic acid will be also studied as a rigid scaffold and it will be compared with the flexible calix[4]arene one. The effect of adsorption amount, dye aggregation and light harvesting ability will be studied and CDCA co-adsorbent will be added to avoid aggregation effect. This further understanding of the molecular characteristics of these dyes will contribute to the design of novel organic sensitizers.

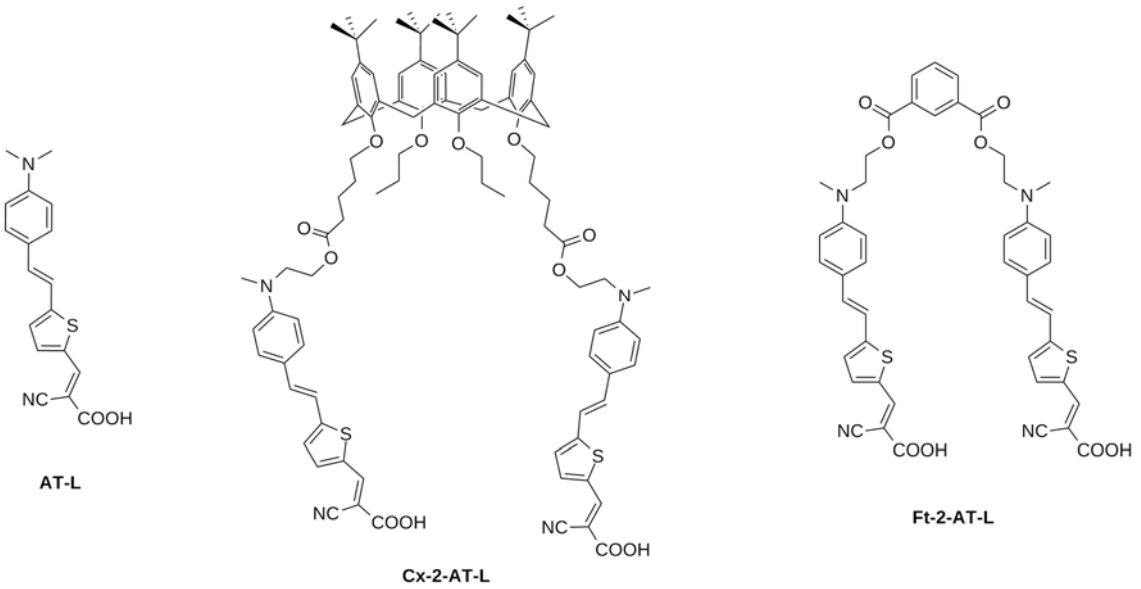

Chart 1. Structures of compounds **AT-L, Cx-2-AT-L, Ft-2-AT-L**

2. Results and discussion

2.1. Synthesis

The **Chart 1** shows the molecular structure of compounds **AT-L, Cx-2-AT-L** and **Ft-2-AT-L**. Hence, **AT-L** is used in this paper to compare its photovoltaic properties with those dibranched difunctionalized derivatives **Cx-2-AT-L** and **Ft-2-AT-L.** All the dyes were characterized by $^{1}H/^{13}C$ NMR spectroscopy, FTIR and mass spectrometry.

Scheme 1 shows the synthesis of the compound **AT-L** which was obtained by a Knoevenagel condensation in chloroform between the formyl group of compound **1**[21] and cyanoacetic acid with piperidine as catalyst in basic media.

The synthesis of compound **3** was carried out following the **Scheme 2.** The *tert*-butyldimethylsilyl group of compound **2** (previously synthesized [22], was removed with tetrabutylammonium fluoride (TBAF) in anhydrous tetrahydrofuran (THF) at room temperature to give with good yield the alcohol derivative **3**.

Scheme 3 and **Scheme 4** depict the preparation of the difunctionalized compounds **Cx-2-AT-L** and **Ft-2-AT-L**, respectively. Dialdehydes **4** and **5** were synthesized, following a method described in the literature [15] by a Steglich reaction of the hydroxyl group of compound **3**, using 1-ethyl-3-(3-dimethylaminopropyl)carbodiimide (EDC), with the corresponding carboxylic acids of the calixarene **Cx-2** [15] and the isophthalic acid, respectively. In the last synthetic step, the acceptor unit was incorporated by a Knoevenagel condensation of the dialdehydes **4** and **5** with cyanoacetic acid and the dianchored dyes **Cx-2-AT-L** and **Ft-2-AT-L** were obtained. It is worthy to note that while compound **AT-L, 2** and **3** consisted of *E/Z* mixtures, **Cx-2-AT-L** and **Ft-2-AT-L** were characterized as *E* only compounds and **AT-L** consisted of a *E/Z* mixture that slowly isomerized to the *E* isomer in solution. This behavior has been already described for analogous donor-acceptor systems bearing strong acceptors. [22]All final organic sensitizers have been characterized.

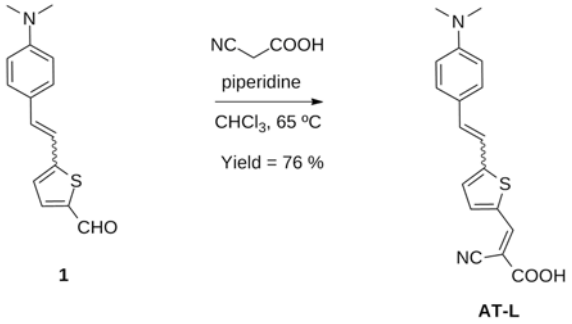

Scheme 1. Synthesis of compound **AT-L**

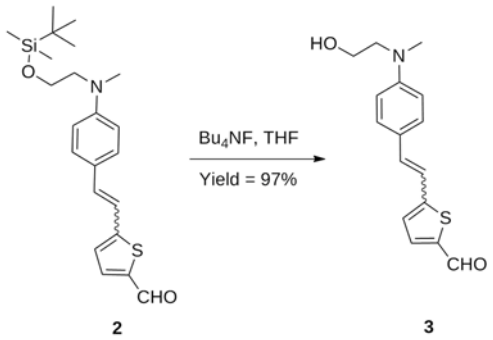

Scheme 2. Synthesis of compound **3**

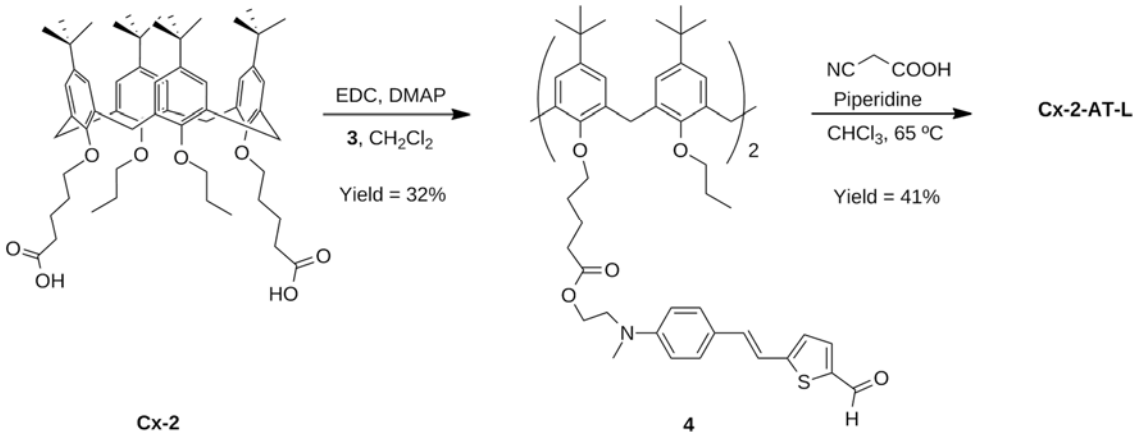

Scheme 3. Synthesis of the compound **Cx-2-AT-L**

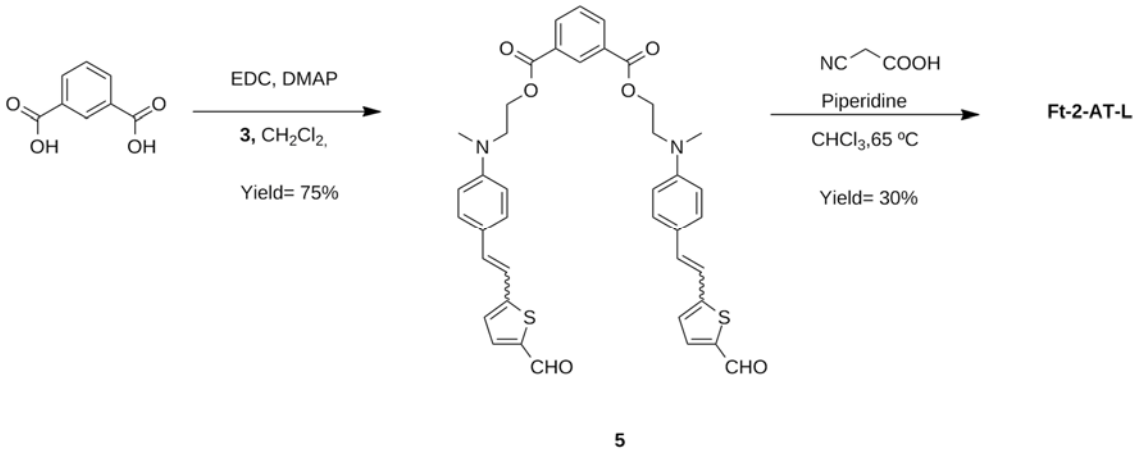

Scheme 4. Synthesis of the compound **Ft-2-AT-L**

2.2. Optical properties

The measurements of UV-vis of the dyes **AT-L**, **Cx-2-AT-L** and **Ft-2-AT-L** have been carried out in 6 10^{-5} M CH_2Cl_2 solution (**Fig. 1**). The spectral range shows a band in the visible region which can be assigned to intramolecular charge transfer (ICT) that occurs between the electron-withdrawing and electron-donating parts of the dyes. [23] Taking into account this broad absorption up to ~ 600 nm and the relatively high absorbance values, quite high short-circuit photocurrent density (J_{sc}) could be expected for the single dye **AT-L** and, especially, for the double derivative **Cx-2-AT-L** [24]

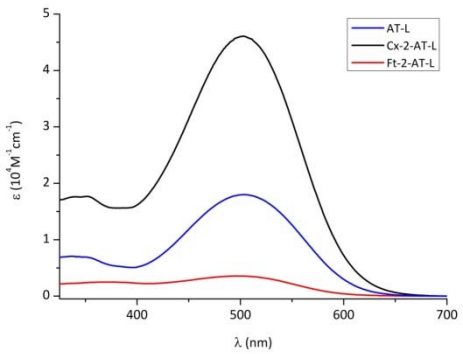

Fig. 1. UV-vis absorption spectra of **AT-L**, **Cx-2-AT-L** and **Ft-2-AT-L** in CH_2Cl_2 (6 × 10^{-5} M).

The molar extinction coefficient of compound **Cx-2-AT-L** with two chromophores in the same scaffold increases (x 2.6) with respect to the individual dye **AT-L**(**Table 1**. Supporting Information, Figure S.2). The enhancement of absorbance per chromophore unit had been observed in previous studies. For instance, a 2.4 increase factor was reported for double dyes with the alkyl linkage in the π-spacer, as **Cx-2-TPA** [20] compared with the single **TPA** [15]. In the present work, with dyes having the alkyl linkage in the donor-part**, Cx-2-AT-L**, the light absorption increase is even greater**.** As the molar extinction coefficient value, ε , is directly related to the amount of radiation which is absorbed by a molecule at a given wavelength, calix[4]arene derivative **Cx-2-AT-L** could have potential applications in low luminosity conditions. [25] However, the compound **Ft-2-AT-L** that also has two chromophores in the same

molecule does not present the same increase of the molar extinction coefficient with respect to **AT-L**. It could be due to intramolecular π-π interactions of the aromatic rings of the two branches of the dye. As it will be discussed in section 2.4, calculations predict that the molecular conformation with the two chromophores very close is somewhat more stable, and low absorption oscillator strength is obtained for this conformation.

Table 1 summarizes the optical properties of the dyes **AT-L**, **Cx-2-AT-L** and **Ft-2-AT-L** in CH_2Cl_2 solution as well as on TiO_2 films.

Table 1. Optical parameters of dyes **AT-L, Cx-2-AT-L, Ft-2-AT-L**

Dye	λ_{abs} [a] (nm)	λ_{abs} [b] (nm)	λ_{corte} (nm)	ε · [a] (10^4 M^{-1}·cm^{-1})
AT-L	502	421	631	1.62±0.05
Cx-2-AT-L	504	429	614	4.25±0.10
Ft-2-AT-L	502	439	607	0.40±0.01

[a]In CH_2Cl_2 solution. [b] Absorption on TiO_2 films.

As concerns the absorption spectra on films, it is known that hypsochromic shifts of the absorption spectra on TiO_2 can be ascribed to deprotonation of the dyes and/or formation of *H*-aggregates (extended head to tail stacking) [26] when dyes are adsorbed on TiO_2 surface. To clarify this point, on the one hand, the UV-vis spectra of **AT-L**, **Cx-2-AT-L** and **Ft-2-AT-L** films were taken after 30 min, 5 h and 24 h of immersion to study aggregation effects (**Fig. 2-4** -left). On the other hand, a series of deprotonation runs [18] were carried out with the three dyes in CH_2Cl_2 solution by addition of an excess amount of triethylamine (**Fig. 2-4.** -right). The hypsochromic shift of the UV-vis spectrum of the three dyes on basic solution with respect to the no basic CH_2Cl_2 solution (60, 54, 58 nm) is attributed to deprotonation effect. [26]

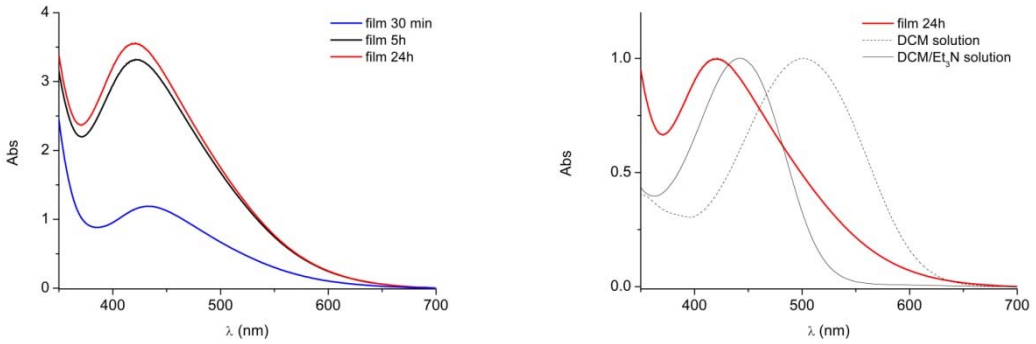

Fig. 2. UV-vis spectra of films (——) prepared with **AT-L** dye after 30 min, 5 and 24 h of immersion (left). The spectra of both CH_2Cl_2 (-----) and CH_2Cl_2/Et_3N solution (——) are also included for showing the effect of the basic solvent on the absorption maximum (right).

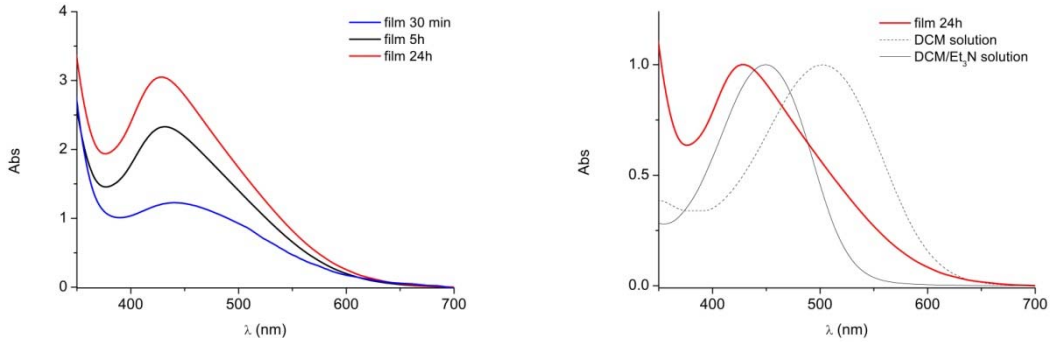

Fig. 3. UV-vis spectra of films (——) prepared with **Cx-2-AT-L** dyes after 30 min, 5 and 24 h of immersion (left). The spectra of both CH_2Cl_2 (-----) and CH_2Cl_2/Et_3N solution (——) are also included for showing the effect of the basic solvent on the absorption maximum (right).

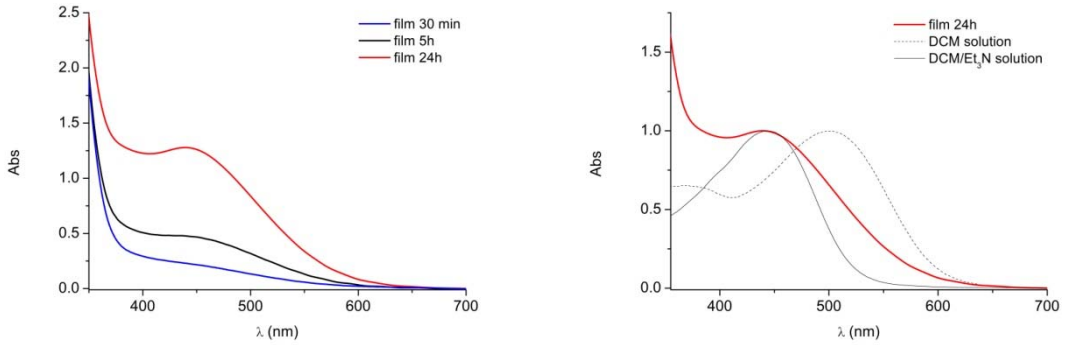

Fig. 4. UV-vis spectra of films (——) prepared with **Ft-2-AT-L** dyes after 30 min, 5 and 24 h of immersion (left). The spectra of both CH_2Cl_2 (-----) and CH_2Cl_2/Et_3N solution (——)are also included for showing the effect of the basic solvent on the absorption maximum (right).

Fig. 2-4-left shows the effect of the adsorption time (from 30 min to 24 h) pointing out that double branched dyes (**Fig. 3, 4-left)** need larger times of adsorption than **AT-L (Fig. 2-left),** probably due to their size. Consequently, the immersion time chosen to perform the devices of these three dyes was 24 h. The UV-vis spectra of the films of **AT-L** and **Cx-2-AT-L** dyes present a blue shift (21 nm and 20 nm, respectively) with respect to the basic solutions, which can be attributed to the effect of the *H*-aggregation. Thus, the two effects seem to play a significant role in the hypsochromic shifting observed for **AT-L** and **Cx-2-AT-L** films as compared with the spectra in solution. However, no significant shift is observed for **Ft-2-AT-L** films as compared with basic solution (**Fig. 4-right)**. This result would point out that there is no relevant *H*-aggregation.

2.3. Electrochemical properties

The electrochemical properties of **AT-L**, **Cx-2-AT-L** and **Ft-2-AT-L** were measured by Differential Pulse Voltammetry (DPV) to know the oxidation potential of both ground and excited states of these dyes, which are listed in **Table 2**. The voltammograms were carried out using 0.1 M Bu_4NPF_6 as supporting electrolyte, a glassy carbon working electrode, a Platinum counter electrode and the Ag/AgCl reference electrode. The voltammograms are reported in the Supporting Information (Figures S.7 and S.9).

Table 2. Transition energy $E_{0\text{-}0}$ and potential values E_{ox} and E_{ox}^*

Dye	E_{ox} vs NHE[a] (V)	$E_{0\text{-}0}$ [b] (eV)	E_{ox}^* [c] (V)
AT-L	+0.92	1.96	-1.04
Cx-2-AT-L	+0.96	2.02	-1.06
Ft-2-AT-L	+0.95	2.04	-1.09

[a] The oxidation potentials were converted to normal hydrogen electrode (NHE) by addition of 0.199 V. [b] $E_{0\text{-}0}$ was estimated from the absorption spectra. [c] The estimated oxidation potential of excited state of the dye was calculated from $E^*_{ox} = E_{ox} - E_{0\text{-}0}$.

The oxidation potential of the dyes **AT-L, Cx-2-AT-L** and **Ft-2-AT-L** is attributed to the oxidation of the donor part of the molecule, the aniline. When dye **AT-L** is compared with a shorter analogue (the 2-cyano-3-(5-(4-(diethylamino)phenyl)thiophen-2-yl)acrylic acid, studied in reference [27]), it can be observed that the longer the π-spacer, the easier the oxidation process (+0,92 V (**AT-L**) vs +1.04 V).

Analysis of the energy levels of sensitizers is very important because dyes must fulfill two electrochemical requirements to perform in DSSCs. (**Table 2**) The oxidation potential of the ground state of the sensitizer must be more positive than the redox potential of the electrolyte (E_{ox} (I_3^-/I^-) = +0.4 V [28]) to ensure that the dye is effectively regenerated after being oxidized. Dyes **AT-L, Cx-2-AT-L** and **Ft-2-AT-L** have similar values of E_{ox} because the aniline fragment is common in all cases. Besides, the oxidation potential of the excited state of the dye must be more negative than the TiO_2 conduction band (E_{ox}^* vs NHE = -0.5 V [29]) to favor the electron injection from the excited dye onto the photoanode and significantly below -0.5 V. The E_{ox}^* values of the dyes **AT-L, Cx-2-AT-L** and **Ft-2-AT-L** do not vary significantly, either. At last, the oxidation potential values of the dyes point out that electron injection and regeneration are energetically permitted. (Supporting Information, Figure S.10).

2.4. Theoretical calculations

In order to get further knowledge of the optical and electrochemical behavior of the studied dyes, we have performed theoretical calculations and the obtained results are gathered in **Table 3**.

Calculations on **AT-L** showed a good agreement to the experimental results for excitation energies (within 0.2 eV), and oxidation potentials (within 0.1 V). The lowest absorption is mainly contributed from a HOMO to LUMO transition with the HOMO and LUMO located on the donor and acceptor part of the chromophore, respectively (**Fig. 5**).

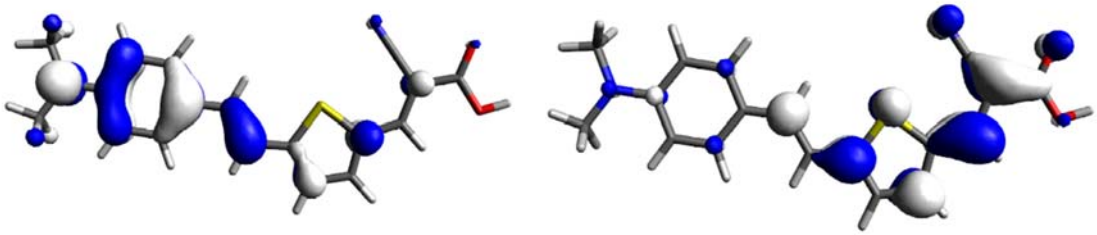

Fig. 5. Contour plots for the HOMO (left) and LUMO (right) of **AT-L (**0.04 isosurface value**)**.

The calculated properties of **Cx-2-AT-L** are those expected for a dichromophoric dye. The absorption spectrum shows two bands at nearly the same wavelength as the observed for the

mono-chromophore dye **AT-L**, but one of them with much higher oscillator strength. It can be explained in the framework of the exciton model which predicts a splitting of the lowest energy absorption into perpendicularly polarized absorptions. [30]

Considering that the low light absorption of **Ft-2-AT-L** may be due in part to intramolecular interactions between chromophores that are possible in this flexible molecule, we have performed calculations on two different conformations: one of them (conformation A) has the chromophores clearly separated while the other (conformation B) allows interchromophore interactions (**Fig. 6**).

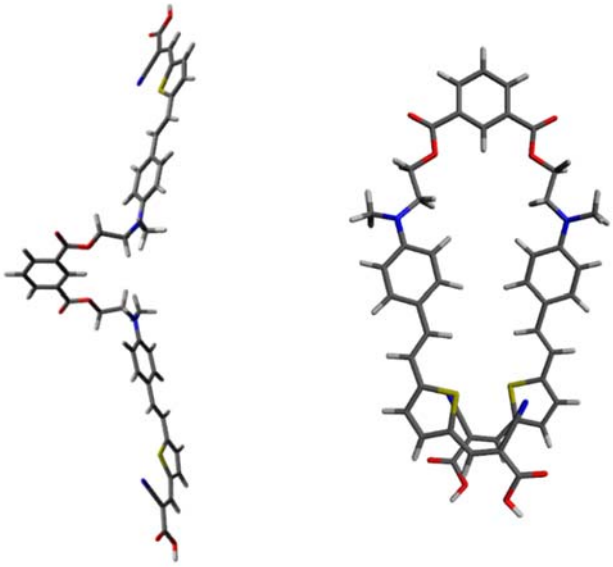

Fig. 6. Optimized geometry of **Ft-2-AT-L** using conformation A (left) and B (right).

The calculations point out that the interchromophore distance is only 3.3 Å in conformation B, and this conformation is more stable than A by only 2.19 Kcal/mol, but the absorption spectra for both conformers are neatly different. The lowest energy absorption for A is calculated at 499 nm with an oscillator strength of 2.86 (almost twice the oscillator strength calculated for the single-chromophore dye **AT-L**) while the spectrum calculated for B shows the lowest energy absorption at 503 nm with an oscillator strength of only 0.59. The second absorption band calculated at 486 nm presents also an oscillator strength lower than conformation A. We can therefore conclude that **Ft-2-AT-L** presents intramolecular interchromophore interactions in its ground state.

Quite surprisingly, we simulated a different behavior for the first excited state and the oxidized radical-cation of **Ft-2-AT-L** resulting in a more stable conformation A compared to B and ruling out interchromophore interactions. The energy differences between these species allow the calculation of the optical and electrochemical parameters (**Table 3**) that compare very precisely to experimental ones in **Table 2**.

Table 3. Calculated[a] parameters for compounds **AT-L**, **Cx-2-AT-L** and **Ft-AT-L**

Dye	E_{HOMO} (eV)	E_{LUMO} (eV)	λ^b (nm)	f	$E_{ox}{}^c$ (V)	$E_{0\text{-}0}$ (eV)	$E^*_{ox}{}^{c,d}$ (V)
AT-L	-6.35	-2.24	512	1.45	1.03	2.16	-1.13
Cx-2-AT-L	-6.45	-2.40	526	2.50	1.14	-	-
			521	0.29			
Ft-2-AT-L	-6.47	-2.26	503	0.59	0.89	1.96	-1.07
			486	1.87			

[a] Calculated using the M06-2x/6-311+G(2d,p) model chemistry and the CPCM solvation model in CH_2Cl_2. [b] Equilibrium CPCM values. [c] Referenced to Normal Hydrogen Electrode (NHE). [d] The oxidation potential of the excited state of the dye was calculated from $E^*_{ox} = E_{ox} - E_{0\text{-}0}$. *f:* oscillator strength.

2.5. Photovoltaic Properties

The results of section **2.3** suggest that conjugated organic compounds based on aniline-thiophene can work irrespective of their scaffold. Here, the influence of the scaffolds, isophthalic acid and calix[4]arene, on device performance and the long-term stability of DSSCs are explored. The preparation of sandwich-type devices was carried out under the following conditions: TiO_2 electrodes were soaked in 0.1 mM dye solutions (CH_2Cl_2) and an electrolyte based on I_3^-/I^- system (0.53 M 1-butyl-3-methylimidazolium iodide, 0.52 M *tert*-butylpyridine, 0.10 M LiI and 0.05 M I_2 in anhydrous acetonitrile) was used.

The optimization of these devices has been carried out by changing the TiO_2 layer thickness. Firstly, devices were prepared with 7 μm thick anodes using 24 h as immersion time (see Supporting Information for details). **Fig. 7** shows both the current–voltage (*J–V*) characteristics and the efficiency of these devices to convert visible light into current in the region 370-700 nm (IPCE). The corresponding photovoltaic parameters are summarized in **Table 4**.

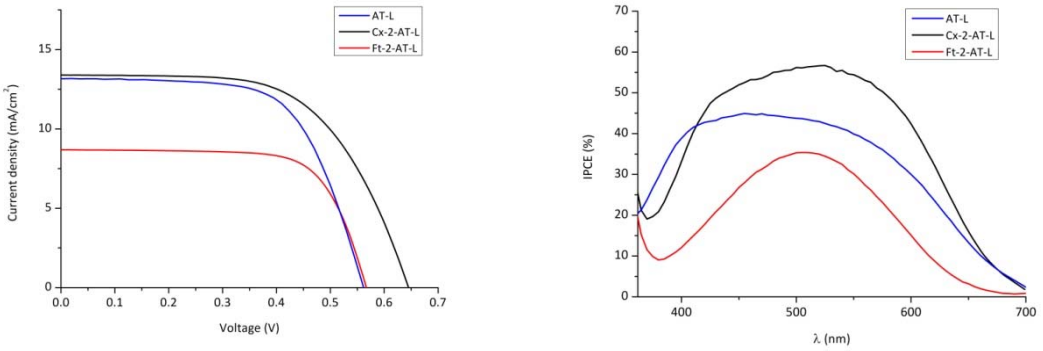

Fig. 7. Current density vs Voltage (left) under AM 1.5 G simulated solar light (100 mW cm^{-2}); b) Incident photon to converted electron efficiency (IPCE) spectra (right) for DSSCs (7 μm thick electrodes) based on the studied dyes (immersion time 24h).

Table 4. Dye loading and average value of the measured photovoltaic parameters: open circuit voltage (V_{oc}), short circuit current density (J_{sc}), fill factor (*ff*) and overall efficiency (η). Three cells of each type were prepared and characterized. Cell area tested: 0.25 cm^2.

Dye	Dye loading *(mol/cm²)*	J_{sc} *(mA/cm²)*	V_{oc} *(V)*	*ff* *(%)*	η *(%)*
AT-L	$3.81\ 10^{-7}$	13.16±0.50	0.568±0.008	63.7±0.2	4.75±0.26
Cx-2-AT-L	$1.19\ 10^{-7}$	13.39±0.27	0.645±0.005	60.3±1.0	5.20±0.23
Ft-2-AT-L	$1.79\ 10^{-7}$	8.69±0.06	0.566±0.003	70.7±0.2	3.50±0.05

Experimental conditions: 7 μm thick electrodes of Dyesol 18NR-AO (paste). 0.1 mM CH_2Cl_2 dye solution, 24 h immersion.

The results in **Table 4** show that the J_{sc} value of **Ft-2-AT-L** is noticeable smaller than that obtained for the single chromophores **AT-L,** which is reflected in the poorest efficiency of the former. The electron injection yield has decreased due to intramolecular interaction between chromophores. As it was mentioned in section **2.2**., it was expected that the dibranched dye **Cx-2-AT-L** would present the best performance. However, the overall efficiency values of the devices prepared with **AT-L** and **Cx-2-AT-L** are not very different, which can be justified because of the lower amount of adsorbed **Cx-2-AT-L** in the electrode, as compared with the corresponding single dye, **AT-L.** Nonetheless, it is noticeable the increase of the V_{oc} in the devices prepared with **Cx-2-AT-L;** this result can be explained due tothe cone scaffold that could inhibit the dark current caused by the recombination of the TiO_2 conduction band electrons with I_3^-. [19, 20, 31, 32]

When dyes with different linkage location are compared, it is observed that the dye loading of the sensitizer with the alkyl linkage on the donor part, **Cx-2-AT-L** ($1.92\ 10^{-7}$),is slightly higher than the loading of dyes with the linkage on the π-spacer, **Cx-2-TPA**($1.30\ 10^{-7}$ mol/cm^2).[19] Moreover, due to the absorption characteristics of these dyes, the IPCE spectrum of the device prepared with **Cx-2-AT-L** is broader than the one of **Cx-2-TPA**. [19]

In order to optimize the performance of these devices, in particular with the aim to improve the **Ft-2-AT-L** properties, 13 μm thick anodes and 24 h as immersion time were used (see Supporting Information for details). Moreover, devices were also prepared with CDCA as co-adsorbent because its use is a common approach in the literature to suppress intermolecular coupling. Two sets of cells were prepared after dye soaking carried out without and with CDCA (0,3 mM); the results of the photovoltaic characterization are depicted in **Fig. 8** and the parameter values are gathered in **Table 5.**

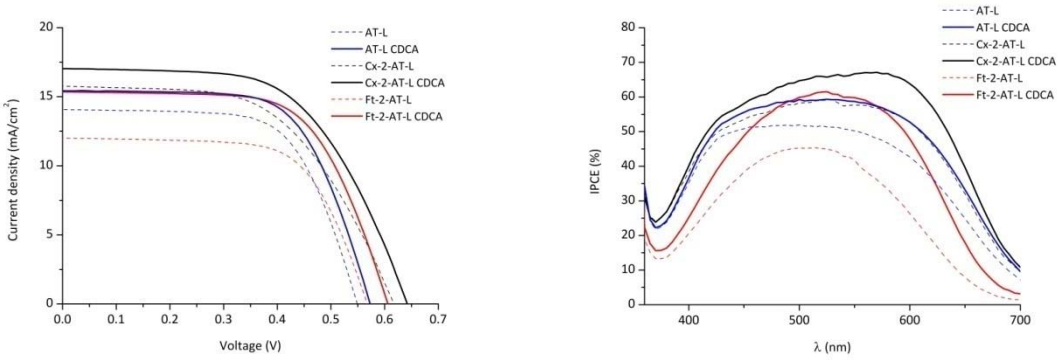

Fig 8. a) Current density vs Voltage (left) under AM 1.5 G simulated solar light (100 mW cm^{-2}); b) Incident photon to converted electron efficiency (IPCE) spectra (right) for DSSCs with (———) and without (- - - -) CDCA (13 μm thick electrodes) based on the studied dyes (immersion time 24 h).

Table 5. Average value of the measured photovoltaic parameters: open circuit voltage (V_{oc}), short circuit current density (J_{sc}), fill factor (*ff*) and overall efficiency (η). Three cells with of each type were prepared and characterized with and without co-adsorbent. The measurements were carried out 24 h after self-assembly. Cell area tested: 0.25 cm^2.

Dye	Co-adsorbent	Dye loading (mol/cm^2)	J_{sc} (mA/cm^2)	V_{oc} (V)	*ff* (%)	η (%)
AT-L	-	$4.85\ 10^{-7}$	14.07±0.17	0.560±0.001	63.9±0.6	5.04±0.11
AT-L	**CDCA**	$3.58\ 10^{-7}$	15.42±0.49	0.583±0.008	64.1±0.8	5.76±0.34
Cx-2-AT-L	-	$2.17\ 10^{-7}$	15.79±0.03	0.616±0.001	55.4±0.1	5.39±0.03
Cx-2-AT-L	**CDCA**	$1.79\ 10^{-7}$	17.07±0.00	0.642±0.001	58.0±0.1	6.35±0.02
Ft-2-AT-L	-	$1.92\ 10^{-7}$	12.01±0.24	0.568±0.007	65.8±0.4	4.49±0.17
Ft-2-AT-L	**CDCA**	$1.95\ 10^{-7}$	15.37±0.45	0.606±0.005	63.9±0.7	5.95±0.30

Experimental conditions: 13 μm thick electrodes of Dyesol 18NR-AO (paste). 0.1 mM CH_2Cl_2 dye solution, 24 h immersion.

The increase of the photoanode thickness resulted in improved overall efficiency. Although somewhat worse values of V_{oc} and *FF* have been obtained for **AT-L** and **CX-2-AT-L** dyes, the increase in J_{sc} is greater, causing the increase in efficiency value **(Tables 4** and **5).** It has been reported for nanosized TiO_2 materials [33] that the increase of photocurrent with increasing film thickness could be attributed to the improved dye loading capacity (due to the higher TiO_2 surface area available for dye adsorption) and light scattering properties.

The addition of the co-adsorbent CDCA is appropriate in every case in spite of the decrease of the loading values observed for **AT-L** and **Cx-2-AT-L**. The increase of the photocurrent and photovoltage values **Fig 8** -left, **Table 5**) is particularly relevant when **Ft-2-AT-L** is used as sensitizer, which means that the aggregates are clearly inhibited. All devices prepared with co-adsorbent improved the V_{oc} because of the reduction of the back electron transfer due to the covering of the photoanode with CDCA. The efficiency of these devices reached values around 6.0 % with the best result for that prepared with calix[4]arene as scaffold that presented a 6.3 % value of efficiency.

Incident photon to converted electron efficiency (IPCE) spectra showed a broad curve (especially

for **Cx-2-AT-L** and **AT-L** based devices) in the visible region up to 700 nm. (**Fig 8** -right). It is known that intense and broad IPCE spectra guarantee high photocurrent and, consequently, good efficiency. The observed increment of J_{sc} values when CDCA is added is clearly reflected in IPCE results, in particular for devices prepared with **Ft-2-AT-L**, which clearly points to the suppression of aggregation. It is verified that control of aggregation and molecular shape are significant issues to improve the performance of devices. [34]

Photovoltaic parameters as a function of time are plotted in **Fig. 9** for devices employing **AT-L, Cx-2-AT-L** or **Ft-2-AT-L** as sensitizers.

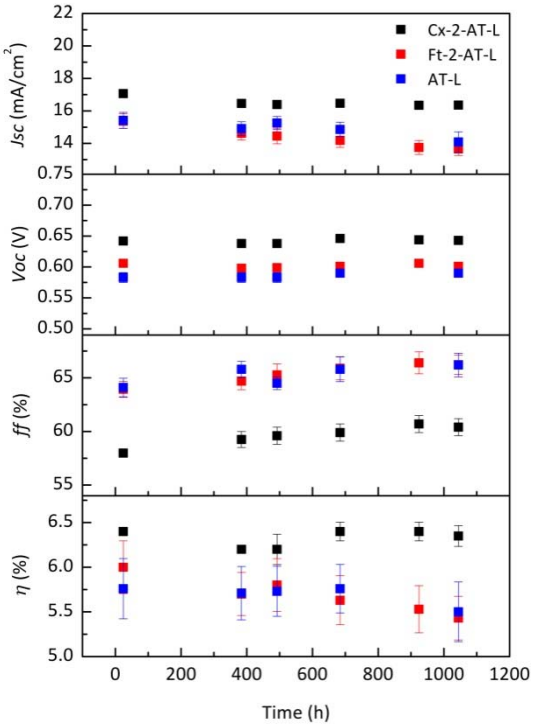

Fig. 9. Temporal evolution of photovoltaic parameters of devices prepared with dyes **AT-L, Cx-2-AT-L** and **Ft-2-AT-L** with CDCA, adsorbed on 13 µm thick photoanodes and after 24 h of immersion time. Measurements were performed under AM 1.5 G simulated solar light (100 mW cm^{-2})

Table 6. Average value of the measured photovoltaic parameters: open circuit voltage (V_{oc}), short circuit current density (J_{sc}), fill factor (*ff*) and overall efficiency (η). Three cells of each type were prepared and characterized (1000 h after cell assembly). Cell area tested: 0.25 cm^2.

Dye	Co-adsorbent	J_{sc} (mA/cm^2)	V_{oc} (V)	*ff* (%)	η (%)
AT-L	-	12.17±0.18	0.590±0.000	65.3±0.7	4.65±0.12
AT-L	**CDCA**	14.09±0.62	0.590±0.000	66.2±1.1	5.50±0.33
Cx-2-AT-L	-	15.04±0.02	0.634±0.002	56.1±0.9	5.35±0.11
Cx-2-AT-L	**CDCA**	16.36±0.04	0.643±0.002	60.4±0.8	6.35±0.12
Ft-2-AT-L	-	10.93±0.32	0.575±0.002	66.6±0.4	4.20±0.16
Ft-2-AT-L	**CDCA**	13.79±0.42	0.602±0.002	66.7±0.5	5.45±0.22

Experimental conditions 13 µm thick electrodes of Dyesol 18NR-AO (paste). 0.1 mM CH_2Cl_2 dye solution, 24 h immersion.

Fig. 9 shows that the devices with calix[4]arene as scaffold are significantly more stable compared to cells with isophthalic acid. The efficiency values of devices prepared with **AT-L** and **Ft-2-AT-L** remains their values between 91-95 % of initial value. However, devices prepared with **Cx-2-AT-L** are essentially stable 1000 h after cell assembly.

Electrochemical Impedance Spectroscopy measurements were performed under illumination (100 mW cm^{-2}) and open-circuit conditions. Devices 13 µm thick were measured, 24 h after assembly). The radius of the intermediate frequency semicircle (the larger one in Figure S.8 – left) in the Nyquist plots represents the charge recombination resistance (R_{rec}) at the TiO_2/dye/electrolyte interface. The resistance decreased in the order of **Cx-2-AT-L > Ft-2-AT-L > AT-L**. The R_{rec} values are 15.32, 11.54, 10.19 Ω, respectively (Figure S.8-left), which are in accordance with the tendency of V_{oc} values (**Table 5**) This result suggests that the recombination of the injected electron with the redox couple in the electrolyte can be inhibited by the use of calix[4]arene as scaffold.
Bode phase plots were used to estimate the lifetime of electrons (τ) (Figure S.8-right) in the conduction band of TiO_2. The electron lifetime was calculated following the equation $\tau = 1/(2\pi f)$ [35] and f is the frequency at the maximum of the curve in the intermediate frequency region of this plot. The τ values were 5.65, 3.31 and 2.60 ms for devices prepared with **Cx-2-AT-L, Ft-2-AT-L** and **AT-L**, respectively. The larger value indicates a reduction of the recombination process on the TiO_2 surface and also supports the tendency of the V_{oc} values.

3.- Conclusions

Among the studied dyes, the one based on calix[4]arene scaffold has the best light harvesting ability, which gives rise to devices with good photovoltaic properties. This scaffold forms a blocking layer between TiO_2 and electrolyte leading a better suppression of the back electron transfer of the injected electrons. Consequently, dyes prepared with this scaffold show the highest V_{oc} values.

The addition of co-adsorbent (**CDCA**) plays a fundamental role for improving the photovoltaic performance, pointing to an effective suppression of aggregation. In particular, J_{sc} values increase for all three dyes, despite the smaller amount of dye adsorbed when **CDCA** is added in **AT-L** and **CX-2-AT-L** based devices. For devices with isophthalic scaffold dye**,** the loading of **Ft-2-AT-L** is essentially the same, and the increase of the overall efficiency is the most remarkable.

As concerns the long-term stability of the devices, the dye-aging tests reveal the remarkable behavior associated with the calix[4]arene scaffold. Specifically, the overall efficiency of devices with **Cx-2-AT-L** remains essentially stable 1000 h after cell assembly.

4.- Experimental Section

<u>(Dimethylamino)thiophene-2-carbaldehyde</u> AT-L

To a solution of cyanoacetic acid (72 mg, 0.22 mmol) and piperidine (275 µL, 2.69 mmol) in dry chloroform (15 mL) a solution of the aldehyde **1** (85.1 mg, 0.33 mmol) was added. The mixture was heated to 70° C of temperature for 48h under argon atmosphere and prevented from light; then it was cooled down to room temperature. The mixture was acidified with HCl 0.1 M (20 ml) and extracted with CH_2Cl_2 (2 x 50 mL). The organic layer was washed with water (3 x 50 mL), dried over magnesium sulfate and the solvent was evaporated by reduced pressure. The resulting solid was triturated with a mixture of cold pentane and few drops of dichloromethane. The final product was isolated as a dark red solid (81.7 mg, 76%).

Molecular weight (g mol^{-1}): 324.3968. **FTIR** (KBr) cm^{-1}: 2213 (C≡N), 1560 (C=O), 3429 (O-H). **Melting point** (°C)**:** 219 **^{1}H-NMR** (400 MHz, DMSO-d^6, 293 K): Isomers *E/Z* 60/30 *E* Isomer 2.96 (s, 6H), 6.71 (d, *J*= 8.8 Hz, 2H), 7.11 (d, *J*= 16 Hz, 1H), 7.26 (d, *J*= 16 Hz, 1H), 7.27 (d, *J*= 4.4 Hz, 1H), 7.48 (d, *J*= 8.8 Hz, 2H), 7.78 (d, *J*= 4.4 Hz, 1H), 8.28 (s, 1H), *Z* Isomer 2.93 (s, 6H), 6.56 (d, *J*= 12 Hz, 1H), 6.66 (d, *J*= 12 Hz, 1H),6.68 (d, *J*= 8.8 Hz, 2H), 7.19 (d, *J*= 4 Hz, 1H), 7.26 (d, *J*= 8.8 Hz, 2H), 7.71 (d, *J*= 4 Hz, 1H), 8.19 (s, 1H). **^{13}C-NMR** (100 MHz, DMSO-d^6, 293K): δ (ppm) 39.7, 111.8, 112.0, 116.0, 116.2, 123.6, 125.4, 128.2, 129.5, 154.7 **HMRS** (ESI^+) m/z: calculated $[C_{18}H_{16}N_2NaO_2S]$:347.0825, found: 347.0824 $[M+Na]^+$. **UV-vis data**λ_{max} (CH_2Cl_2) (nm): 502, molar extinction coefficient ε_{max}(M^{-1} cm^{-1}): 16200±500

5-(4-((2-hydroxyethyl)(methyl)amino)styryl)thiophene-2-carbaldehyde 3

To a solution of compound **2** previously synthesized [17] (180 mg, 0.45 mmol) in THF at 0°C of temperature under Argon, a solution of tetrabutylammonium fluoride (1M in THF) (0.9 mL, 0.9 mmol) was slowly added and was stirred for 90 min. The resulting solution was quenched by the addition of 40 mL of H_2O and 100 mL of NH_4Cl saturated solution (aq). The aqueous phase was extracted with ethyl acetate solution (3x60 mL) and the organic phase was dried over dry $MgSO_4$ and the solvent was evaporated by reduced pressure. The residue was purified by flash chromatography (hexane/ethyl acetate 1:1) and the final product was isolated as red solid (127 mg, 97%).

Molecular weight (g/mol): 287. **FTIR** (KBr) cm^{-1}: 1640 (C=O), 2918 (C-H), 3505 (O-H) **Melting point** (^{o}C): 151 **^{1}H- NMR** (400 MHz, CD_2Cl_2) δ (ppm): mixture *E/Z* 80/20. *E* Isomer: 3.03 (s, 3H), 3.50-3.54 (m, 2H), 3.86 (t, *J*= 5.6 Hz, 2H), 6.76 (d, *J*= 8.8 Hz, 2H), 7.03 (d, *J*=16 Hz, 1H), 7.08-7.13 (m, 2H), 7.39 (d, *J*=8.8 Hz, 2H), 7.65 (d, *J*=4 Hz, 1H), 9.79 (s, 1H). *Z* Isomer: 3.01 (s, 3H), 3.50-3.54 (m, 2H), 3.86 (t, *J*= 5.6 Hz, 2H), 6.53 (d, *J*= 12 Hz, 1H), 6.70 (d, *J*= 12 Hz, 1H), 6.76 (d, *J*= 8.8 Hz, 2H), 7.08-7.13 (m, 1H), 7.25 (d, *J*= 8.8 Hz, 2H), 7.58 (d, *J*= 4 Hz, 1H), 9.77 (s, 1H). **^{13}C- NMR** (100 MHz, CD_2Cl_2): 39.1, 39.2, 55.3, 55.4, 60.7, 112.7, 112.9, 116.7, 124.6, 125.8, 128.9, 130.5, 133.9, 134.8, 138.2, 140.9, 150.9, 154.4, 182.8**. HMRS** (ESI^+) m/z: calculated for $[C_{16}H_{18}NO_2S]^+$: 288.1053, found 288.1050 $[M+H]^+$.

Calix[4]arene derivative of 3, dialdehyde 4

To a solution of calixarene diacid **Cx-2** (146 mg, 0.16mmol) in anhydrous dichloromethane, 4-dimethylaminopyridine (DMAP) (24 mg, 0.19 mmol) and 1-ethyl-3-[3-dimethylaminopropyl]carbodiimide hydrochloride (EDC) (284 mg, 1.48 mmol) were successively added. This mixture was maintained at 0 °C during 30 min. Alcohol **3** (90 mg, 0.31mmol) was added. The reaction mixture was then stirred at room temperature for 5 days. Then it was washed and dried over magnesium sulfate and the solvent was evaporated by reduced pressure. The residue was purified by flash chromatography with variable polarity using hexane/ethyl acetate with polarity from (8:2) to (6:4). The desired product that was isolated as an orange oil (76 mg, 32%).

Molecular weight (g/mol): 1472. **FTIR** (NaCl) cm^{-1}: 1662 (C=O), 1733 (C=O), 2868, 2960 (C-H). **Melting point** (^{o}C): 102 **^{1}H- NMR** (300 MHz, CD_2Cl_2) δ (ppm): mixture *E/Z* 90/10. *E* isomer: 0.97 (t, *J*= 7.5 Hz, 6H), 1.06 (s, 18H), 1.09 (s, 18H), 1.73 (q, *J*= 5.8 Hz, 4H), 1.94-2.07 (m, 8H), 2.37 (t, *J*= 7.8 Hz, 4H), 3.01 (s, 6H), 3.11 (d, *J*= 12.6 Hz, 4H), 3.63 (t, *J*= 6 Hz, 4H), 3.76-3.85 (m, 8H), 4.26 (t, *J*= 6 Hz, 4H), 4.36 (d, *J*= 12.6 Hz, 4H), 6.71 (d, *J*= 8.7 Hz, 4H), 6.77 (s, 4H), 6.81 (s, 4H), 7.00 (d, *J*= 15.9 Hz, 2H), 7.07 (d, *J*= 4.2 Hz, 2H), 7.10 (d, *J*= 15.9 Hz, 2H), 7.37 (d, *J*= 8.7 Hz, 4H), 7.64 (d, *J*= 4.2 Hz, 2H), 9.80 (s, 2H). *Z* isomer: 0.97 (t, *J*= 7.5 Hz, 6H), 1.06 (s, 18H), 1.09 (s, 18H), 1.73 (q,

J= 5.8 Hz, 4H), 1.94-2.07 (m, 8H), 2.37 (t, *J*= 7.8 Hz, 4H), 3.01 (s, 6H), 3.11 (d, *J*= 12.6 Hz, 4H), 3.63 (t, *J*= 6 Hz, 4H), 3.76-3.85 (m, 8H), 4.26 (t, *J*=6 Hz, 4H), 4.36 (d, *J*= 12.6 Hz, 4H), 6.50 (d, *J*= 12 Hz, 2H), 6.66 (d, *J*= 8.7 Hz, 4H), 6.77 (s, 4H), 6.78 (d, *J*= 12 Hz, 2H), 6.81 (s, 4H), 7.07 (d, *J*= 4.2 Hz, 2H), 7.24 (d, *J*= 8.7 Hz, 4H), 7.56 (d, *J*= 4.2 Hz, 2H), 9.77 (s, 2H). **^{13}C-NMR** (100 MHz, CD_2Cl_2): 10.7, 22.2, 24.0, 30.3, 31.6, 31.8, 31.8, 33.4, 34.7, 39.1, 51.4, 61.8, 75.2, 77.5, 112.6, 116.8, 125.6, 125.8, 129.0, 133.8, 134.3, 134.5, 138.2, 144.9, 154.0, 154.3, 173.7, 182.8 **MS** (MALDI$^+$) m/z: calculated for $[C_{92}H_{114}N_2O_{10}S_2Na]^+$: 1493.8 found 1494.1 $[M+Na]^+$.

Dye Cx-2-AT-L

To a solution of the dialdehyde **4** (67 mg, 0.046 mmol) and cyanoacetic acid (19 mg, 0.23 mmol) in chloroform (10 ml), piperidine (71 µL, 0.7 mmol) was added. The mixture was heated to 65^{o}C of temperature for 2 days under argon atmosphere and prevented from light; then it was cooled down to room temperature. The mixture was acidified with HCl 0.1 M (10 mL) and was stirred vigorously for 30 min. Then it was extracted with CH_2Cl_2 (2 x 50 mL). The organic layer was washed with water (3 x 50 mL), dried over magnesium sulfate and the solvent was evaporated by reduced pressure. The resulting solid was triturated with cold MeOH. The final product was isolated as dark red solid (32 mg, 41 %).

Molecular weight (g/mol): 1606. **FTIR** (KBr) cm^{-1}: 1603 (C=C), 1729 (C=O), 2212 (C Ξ N), 3402 (O-H) **Melting point** (^{o}C): 155 **^{1}H- NMR** (400 MHz, THF-d^8) δ (ppm): 0.99 (t, *J*= 7.2 Hz, 6H), 1.08 (s, 18H), 1.10 (s, 18H), 1.75-1.79 (m, 4H), 1.97-2.05 (m, 8H), 2.37 (t, *J*= 7.2 Hz, 4H), 3.02 (s, 6H), 3.11 (d, *J*= 12.6 Hz, 4H), 3.64-3.67 (m, 4H), 3.79-3.85 (m, 8H), 4.26 (t, *J*= 6 Hz, 4H), 4.41 (d, *J*= 12.6 Hz, 4H), 6.74 (d, *J*= 9 Hz, 4H), 6.80 (s, 4H), 6.84 (s, 4H), 7.12-7.14 (m, 6H), 7.40 (d, *J*= 9 Hz, 4H), 7.70 (d, *J*= 4 Hz, 2H), 8.26 (s, 2H). **^{13}C- NMR** (100 MHz, THF-d^8): 10.9, 24.4, 30.8, 30.9, 32.0, 32.1, 34.6, 34.8, 39.0, 51.6, 62.2, 75.8, 75.9, 98.6, 113.0, 117.1, 125.6, 126.0, 126.4, 129.5, 134.6, 134.7, 134.8, 135.0, 140.3, 145.1, 146.5, 150.8, 154.7, 154.9, 155.3, 164.6, 173.5. **MS** (MALDI$^+$) m/z: calculated for $[C_{98}H_{116}N_4O_{12}S_2]^{+\bullet}$: 1604.8 found 1605.0 $[M]^{+\bullet}$. **UV-vis data** λ_{max} (CH_2Cl_2) (nm): 504, molar extinction coefficient ε_{max}(M^{-1} cm^{-1}): 42500 ± 1000.

Ftalate derivative of 3, dialdehyde 5

To a solution of isophthalic acid **Ft-2** (23 mg, 0.14 mmol) in anhydrous dichloromethane, 4-dimethylaminopyridine (DMAP) (8 mg, 0.07 mmol) and 1-ethyl-3-[3-dimethylaminopropyl]carbodiimidehydrochloride (EDC) (96 mg, 0.5 mmol) were successively added. This mixture was maintained at 0 °C during 30 min. Alcohol **3** (80 mg, 0.31 mmol) was added. The reaction mixture was then stirred at room temperature for 3 days. Then it was washed and dried over magnesium sulfate and the solvent was evaporated by reduced pressure. The residue was purified by flash chromatography using dichloromethane, hexane/ethyl acetate and CH_2Cl_2/ethyl acetate (95:05), successively. The desired product that was isolated as an orange oil (73 mg, 75%).

Molecular weight (g/mol): 705. **FTIR** (NaCl) cm^{-1}: 1653 (C=O) **Melting point** (^{o}C): 110 **^{1}H-NMR** (300 MHz, CD_2Cl_2) δ (ppm): mixture *E/Z* 68/32 *E* isomer: 3.08 (s, 6H), 3.76-3.82 (m, 4H), 4.53 (t, *J*= 5.7 Hz, 4H), 6.78 (d, *J*= 9 Hz, 4H), 7.01 (d, *J*= 16.2 Hz, 2H), 7.08 (d, *J*= 4 Hz, 2H), 7.10 (d, *J*= 16.2 Hz, 2H), 7.39 (d, *J*= 9 Hz, 4H), 7.46-7.54 (m, 1H), 7.65 (d, *J*= 4 Hz, 2H), 8.12 (dd, *J*= 7.8 Hz, *J*= 1.8 Hz, 2H), 8.55-8.59 (m, 1H), 9.81 (s, 2H) *Z* isomer: 3.08 (s, 6H), 3.76-3.82 (m, 4H), 4.53 (t, *J*= 5.7 Hz, 4H), 6.52 (d, *J*= 12 Hz, 2H), 6.68 (d, *J*= 12 Hz, 2H), 6.78 (d, *J*= 9 Hz, 4H), 7.08 (d, *J*= 4 Hz, 2H), 7.26 (d, *J*= 9 Hz, 4H), 7.46-7,54 (m, 1H), 7.56 (d, *J*=4 Hz, 2H), 8.13 (dd, *J*= 7.8 Hz, *J*= 1.8 Hz, 2H), 8.55-8.59 (m, 1H), 9.77 (s, 2H). **^{13}C-NMR** (75 MHz, CD_2Cl_2): 39.1, 51.4, 63.0, 112.4, 112.8, 116.9, 120.1, 124.8, 125.8, 129.0, 129.1, 129.3, 130.6, 131.1, 131.2, 133.8, 134.3, 134.8, 136.9, 138.2,

141.0, 150.2, 154.3, 166.1, 182.8, 183.2 HRMS (ESI$^+$) m/z: calculated for $[C_{40}H_{36}N_2O_6S_2Na]^+$: 727.1907 found 727.1936 $[M+Na]^+$.

Dye Ft-2-AT-L

To a solution of the dialdehyde 5 (62 mg, 0.088 mmol) and cyanoacetic acid (22 mg, 0.26 mmol) in chloroform (10 ml), piperidine (119 µL, 1.16 mmol) was added. The mixture was heated to 65 ^oC of temperature for 24 hours under argon atmosphere and prevented from light; then it was cooled down to room temperature. The mixture was acidified with HCl 0.1 M (25 mL) and was stirred vigorously for 30 min. Then it was extracted with CH_2Cl_2 (2 x 50 mL). The organic layer was washed with water (3 x 50 mL), dried over magnesium sulfate and the solvent was evaporated by reduced pressure. The resulting solid was triturated with cold CH_2Cl_2/MeOH. The final product was isolated as maroon solid (22 mg, 30 %).

Molecular weight (g/mol): 839 **FTIR** (KBr) cm^{-1}: 1725 (C=O), 1598 (C=C), 2212 (C≡N), 3383 (O-H) **Melting point** (^{o}C): >350 **^{1}H-NMR** (300 MHz, THF-d^8) δ (ppm): 3.08 (s, 6H), 3.82 (t, *J*= 5.6 Hz, 4H), 4.52 (t, *J*= 5.6 Hz, 4H), 6.82 (d, *J*= 8.8 Hz, 4H), 7.13-7.15 (m, 6H), 7.44 (d, *J*= 8.8 Hz, 4H), 7.50 (t, *J*= 7.8 Hz, 1H), 7.70 (d, *J*= 4 Hz, 2H), 8.11 (d, *J*= 7.8 Hz, 2H), 8.27 (s, 1H), 8.58 (s, 2H), 10.83 (s, 2H). **^{13}C-NMR**: insoluble **HRMS** (ESI$^+$) m/z: calculated for $[C_{46}H_{39}N_4O_8S_2]$: 839.2204 found 839.2182 $[M+H]^+$. **UV-vis data** λ_{max} (CH_2Cl_2) (nm): 502, molar extinction coefficient ε_{max} (M^{-1} cm^{-1}): 4000 ± 100.

Acknowledgements

We gratefully acknowledge the financial support from the Universidad de Zaragoza (UZ2019-CIE-01), the Spanish Ministry of Science and Innovation-MICINN-FEDER (Project CTQ2014–52331-R) and Gobierno de Aragón-Fondo Social Europeo (E14-17R and E47-20R). ID and DB acknowledge for the financial support of Gobierno de Aragón fellowship and PhD studentship Santander-2018 programs, respectively. Moreover, anonymous referees are gratefully acknowledged for helpful suggestions.

REFERENCES

[1] Extance A. Perovskites on trial. Nature 2019; 570: 429-32. https://doi.org/10.1038/d41586-019-01985-y

[2] Vougioukalakis GC, Philippopoulos A, Stergiopoulos T, Falaras P. Contributions to the development of ruthenium-based sensitizers for dye-sensitized solar cells. Coord Chem Rev 2010; 255:2602-21. https://doi.org/10.1016/j.ccr.2010.11.006

[3] Ji J-M, Zhou H, Kim H K. Rational design criteria for D–π–A structured organic and porphyrin sensitizers for highly efficient dye-sensitized solar cells. J Mater Chem A 2018; 6:14518-45. https://doi.org/10.1039/c8ta02281j

[4] Ho C-L, Wong W-Y. High performance arylamine-based metallated and metal-free organic photosensitizers for dye-sensitized solar cells. J Photochem Photobiol C 2016; 28: 138–58. https://doi.org/10.1016/j.jphotochemrev.2016.05.002

[5] Liang M, Chen J. Arylamine organic dyes for dye-sensitized solar cells. Chem Soc Rev 2013; 42: 8, 3453-88. https://doi.org/10.1039/c3cs35372a

[6] Duerto I, Colom E, Andrés JM, Franco S, Garín J, Orduna J, Villacampa B, Blesa MJ. DSSCs based on aniline derivatives functionalized with a tert-butyldimethylsilyl group and the effect of the π–spacer. Dyes Pigm 2018; 148: 61-71. https://doi.org/10.1016/j.dyepig.2017.07.063

[7] Chaurasia S, Liang, C-J, Yen, Y-S, Lin J T. Sensitizers with rigidified-aromatics as the conjugated spacers for dye-sensitized solar cells. J Mater Chem 2015; 38: 9765-9780. https://doi.org/10.1039/c5tc02356d

[8] Chen, Y-C, Lin, J T. Multi-anchored sensitizers for dye-sensitized solar cells. Sustainable Energy Fuels 2017;1: 969–985. https://doi.org/10.1039/c7se00141j
[9] Numata Y, Islam A, Chen H, Han L. Aggregation-free branch-type organic dye with a twisted molecular architecture for dye-sensitized solar cells. Energy Environ Sci, 2012, 5: 8548–52. https://doi.org/10.1039/C2EE22506A
[10] Otsuka A, Funabiki K, Sugiyama N, Mase H, Yoshida T, Minoura H, Matsui M. Design and synthesis of Near-infrared-active Heptamethine–Cyanine Dyes to Suppress Aggregation in a Dye-sensitized Porous Zinc Oxide Solar Cell. Chem. Lett., 2008, 37: 176–7.https://doi.org/10.1246/cl.2008.176
[11] Kryman M W, Nasca J N, Watson D F, Detty M R. Selenorhodamine Dye-Sensitized Solar Cells: Influence of Structure and Surface-Anchoring Mode on Aggregation, Persistence, and Photoelectrochemical Performance. Langmuir, 2016, 32: 1521–32. https://doi.org/10.1021/acs.langmuir.5b04275
[12] Matsuzaki H, Murakami T N, Masaki N, Furube A, Kimura M, Mori S. Dye Aggregation Effect on Interfacial Electron-Transfer Dynamics in Zinc Phthalocyanine-Sensitized Solar Cells. J Phys Chem C, 2014, 118: 17205-12. https://doi.org/10.1021/jp500798c
[13] Zhang L, Cole J M. Dye aggregation on dye-sensitized solar cells. J Mater Chem A 2017; 5: 19541-59. https://doi.org/10.1039/C7TA05632J
[14] Cao D, Peng J, Hong Y, Fang X, Wang L, Meier H. Enhanced Performance of the Dye-Sensitized Solar Cells with Phenothiazine-Based Dyes Containing Double D−A Branches. Org Lett 2011;13: 1610–13. https://doi.org/10.1021/ol2000167
[15] Castillo-Vallés M, Andrés-Castán JM, Garín J, Orduna J, Villacampa B, Franco S, Blesa M J. Dye-sensitized-solar-cells based on calix[4]arene scaffold. RSC Adv 2015; 5: 90667-70. https://doi.org/10.1039/c5ra15184h
[16] Zang X-F, Zhang T L, Huang Z S, Iqbal Z, Kuang D B, Wang L, Meier H, Cao D. Impact of the position isomer of the linkage in the double D-A branch-based organic dyes on the photovoltaic performance. Dyes Pigm 2014; 104: 89–96. https://doi.org/10.1016/j.dyepig.2013.12.028
[17] Jiang S, Fan S, Lu X, Zhou G, Wang Z-S. Double D-π-A branched organic dye isomers for dye-sensitized solar cells. J Mater Chem A 2014; 2: 17153-64.
https://doi.org/10.1039/C4TA03451A
[18] Huang Z-S, Cai C, Zang X-F, Iqbal Z, Zeng H, Kuang D-B, Wang L, Meier H, Cao D. Effect of the linkage location in double branched organic dyes on the photovoltaic performance of DSSCs . J Mater Chem A 2015; 3: 1333–44. https://doi.org/10.1039/c4ta05652c
[19] Colom E, Andres J M, Franco S, Garín J, Montoya J F, Orduna J, Villacampa B, Blesa M J. Multichromophoric sensitizers based on calix[4]arene scaffold and *4H*-pyranylidene moiety for DSSCs application. Dyes Pigm 2017; 136: 505-14. http://dx.doi.org/10.1016/j.dyepig.2016.08.067
[20] Colom E, Andrés-Castán J M, Barrios D, Duerto I, Franco S, Garín J, Orduna J, Villacampa B, Blesa M J. Modification of the electronic properties of the π-spacer of chromophores linked to calix[4]arene platform for DSSCs applications. Dyes Pigm 2019; 164: 43–53. https://doi.org/10.1016/j.dyepig.2018.12.066
[21] Duerto I, García-Palacín M, Barrios D, Garín J, Orduna J, Villacampa B, Blesa MJ. A novel s-linkage to dianchor dyes for efficient dyes sensitized solar cells. Dyes Pigm 2020; 173: 107945. https://doi.org/10.1016/j.dyepig.2019.107945
[22] González-Laínez M, Jiménez-Ruiz MT, Martínez de Baroja N, Garín J, Orduna J, Villacampa B, Blesa MJ. Using functionalized nonlinear optical chromophores to prepare NLO-active polycarbonate films. Dyes Pigm 2015; 119:30-40.http://dx.doi.org/10.1016/j.dyepig.2015.02.026
[23] Roquet S, Cravino A, Leriche P, Alévêque O, Frère P, Roncali J, Triphenylamine−Thienylenevinylene Hybrid Systems with Internal Charge Transfer as Donor Materials for Heterojunction Solar Cells. J Am Chem Soc 2006; 128: 3459-66.

https://doi.org/10.1021/ja058178e
[24] Chen Y-C, Lin J-T. Multi-anchored sensitizers for dyes-sensitizers solar cells. Sustainable Energy Fuels 2017; 1:969-85. https://doi.org/10.1039/C7SE00141J
[25] Vaghasiya J V, Sonigara K K, Suresh L, Panahandeh-Fard M, Soni S S, Tan S C. Efficient power generating devices utilizing low intensity indoor lights via non-radiative energy transfer mechanism from organic ionic redox couples. Nano Energy 2019; 60: 457–66. http://dx.doi.org/10.1016/j.nanoen.2019.03.086
[26] Nüesch F, Gratzel M. *H*-aggregation and correlated absorption and emission of a merocyanine dye in solution, at the surface and in the solid state. A link between crystal structure and photophysical properties. Chem Phys 1995; 193: 1-17. http://dx.doi.org/10.1016/0301-0104(94)00405-Y
[27] Parka S W, Sona K-I, Koa M J, Kima K, Park N-G. Effect of donor moiety in organic sensitizer on spectral response, electrochemical and photovoltaic properties. Synthetic Metals 2009; 159: 2571–7. https://doi.org/10.1016/j.synthmet.2009.09.013
[28] Hagfeldt A, Grätzel M. Light-Induced Redox Reactions in Nanocrystalline Systems. Chem Rev 1995; 95:49–68.https://doi.org/10.1021/cr00033a003
[29] Pazoki M, Cappel UB, Johansson EMJ, Hagfeldt A, Boschloo G. Characterization techniques for dye-sensitized solar cells. Energy Environ Sci 2017; 10: 672–709. https://doi.org/10.1039/c6ee02732f
[30] Andreu R, Franco S, Garín J, Romero J, Villacampa B, Blesa MJ, Orduna J. Multichromophoric calixarenes: Effect of interchromophore distances on linear and nonlinear optical properties. ChemPhysChem, 2012; 13:3204-9. https://doi.org/10.1002/cphc.201200203
[31] Tan L-L, Liu K-M, Li S-Y, Xiao L-M, Kuang D-B, Su C-Y. Dye-Sensitized Solar Cells with Improved Performance using Cone-Calix[4]Arene Based Dyes. ChemSusChem 2015; 8: 280 – 7. https://doi.org/10.1002/cssc.201402401
[32] Hua T, Zhang K, Huang Z-S, Wang L, Tang H, Meier H, Cao D. Effect of structural engineering of π-spacers on anti-aggregation of D–A–π–A dyes. J Mater Chem C 2019; 7: 10379-88. http://dx.doi.org/10.1039/C9TC03066B

[33] Wu X, Lu G, Wang L. The effect of photoanode thickness on the performance of dye-sensitized solar cells containing TiO_2 nanosheets with exposed reactive {001} facets. J Mater Res 2013, 28: 475-9. http://dx.doi.org/10.1557/jmr.2012.372
[34] Wu Y, Zhang Q, Li J, Tian X, Li D, Lu X, Xu B, Wu Y, Guo K. Regulation of dithiafulvene-based molecular shape and aggregation on TiO_2 for high efficiency dye-sensitized solar cells. J. Mater Chem C 2019; 7: 1974-81. https://doi.org/10.1039/c8tc06109b
[35] Kern R, Sastrawan R, Ferber J, Stangl R, Luther J. Modeling and interpretation of electrical impedance spectra of dye solar cells operated under open-circuit conditions. Electrochim Acta 2002; 47: 4213–25. https://doi.org/10.1016/S0013-4686(02)00444-9